Microstructural evolution and mechanical properties of in-situ as-cast beta titanium matrix composites

Vitor V. Rielli[a], Vicente Amigó-Borrás[b], Rodrigo J. Contieri[a]

[a] University of Campinas, School of Applied Sciences, 13484-350, Limeira, Brazil.

[b] Institute of Materials Technology, Polytechnic University of Valencia, 22012, Valencia, Spain.

Abstract

The aim of this research is to investigate the effects of B_4C additions on microstructure refinement and mechanical properties, due to in-situ formation of TiB and TiC in a matrix of beta titanium by casting process. Research has been done on the effects of TiC and TiB compounds on titanium composites, however their hybrid effect has been scarcely explored on beta titanium alloys. The effects on lattice parameter were investigated by Rietveld refinement and EDS analysis. The beta lattice parameters increased due reaction between Ti and B_4C. DTA analysis revealed the sequence of phase formation on heating and cooling around the melting point, being confirmed by investigation of orientation relationship between phases by EBSD and pole figure analysis. Orientation relationships are $\{312\}_{TiB}//\{112\}_{\beta}$, $\{112\}_{TiC}//\{112\}_{\beta}$ for the lowest composition of B_4C, $\{113\}_{TiC}//\{112\}_{\beta}$ for the remaining composites, and $\{010\}_{TiB}//\{011\}_{TiC}$ between the particles. Grain size reduced by half with 0.5% addition of B_4C, while 3% made grains 25 times smaller than the alloy. Young's modulus and hardness of the beta phase increased with addition of boron carbide. The as-cast composite materials have a refined structure with improved mechanical properties in comparison to the commercial alloy.

Keywords

Titanium matrix composite; As-cast; Beta 21S; TiB; TiC.

Declaration of interest: none

1. Introduction

Beta titanium alloys have been studied as efficient matrix materials for composites with different volumes of reinforcement [1-4]. TIMETAL 21S (Ti-15Mo-3Nb-3Al-0.2Si, wt.%) is a metastable beta titanium alloy developed for having good properties as matrix for composites aiming high temperature applications, being currently employed at the plug-and-nozzle segment of aircraft engines [5].

To improve alloy thermal stability in operation temperatures ranging from 500 to 600°C, several thermomechanical processing steps must be carried out to refine grains from casting, including forging, annealing, and single or duplex aging, which significantly increases manufacturing costs [6-8]. Phase precipitation of discontinuous reinforcements such as TiB and TiC has been shown to decrease grain coarsening during solidification from the melt, acting as pinning particles [9-11]. These borides and carbides can be formed from in-situ reactions with titanium when B_4C is added to the material subjected to melting techniques. A ratio of four TiB for each TiC results from the following reaction [12]:

$$5Ti + B_4C \rightarrow 4TiB + TiC \qquad (1)$$

For similar beta metastable titanium alloys as the one used in this research, the cooling rate in vacuum arc remelting (VAR) can be fast enough to completely retain the metastable beta phase at room temperature [13,14]. Owing to its bcc crystal structure, beta phase matrix has low mechanical properties that can be improved when fine precipitates are formed, such as alpha phase, but also intermetallic in-situ components like TiB and TiC. Increase in hardness and elastic modulus is expected for composites with high volumes of these reinforcements [15,16].

Researches have investigated the individual effects of TiB and TiC precipitation in materials based on Ti CP, alpha, and alpha + beta titanium alloys [17-20], however, their hybrid effect has been scarcely explored on beta titanium alloys, especially on as-cast condition [21]. In the

present work, the beta titanium alloy Beta 21S is used as matrix material for composites with different concentrations of B_4C, forming up to 20.7% of volume of in-situ reinforcements. Effects on lattice parameter and microstructure of as-cast condition are discussed in light of Rietveld refinement and SEM images, as well as the variation of mechanical properties such as Young's modulus and hardness from nano to macro level. A study of orientation relationship associated with differential thermal analysis (DTA) allowed a better understanding of the sequence of phase formation during melting and solidification. Improving mechanical properties, achieving a refined and homogeneous microstructure straight from the cast means a significant reduction in further processing steps, decreasing production costs.

2. Experimental Procedure

Based on the Ti-B_4C isopleth [22], and knowing from the Ti-B [23] and Ti-C [24] phase diagrams that the eutectic composition of B and C in Ti is 7±1 at. %B and 1.32 at. %C, three additions of B_4C to Beta 21S (84.29Ti-8Mo-5.69Al-1.65Nb-0.36Si, at.%) were selected. AC0.5 is lower than eutectic for both B and C with 0.5 wt.% of B_4C (82.28Ti-7.86Mo-5.59Al-1.62Nb-0.36Si-1.86B-0.42C, at.%); AC1.5 has composition near eutectic for both elements, with 1.5 wt.% of B_4C (78.48Ti-7.6Mo-5.4Al-1.57Nb-0.35Si-5.39B-1.21C, at.%); and AC3 is hypereutectic with 3 wt.% of B_4C (73.23Ti-7.23Mo-5.14Al-1.49Nb-0.33Si-10.27B-2.31C, at.%). A Beta 21S ingot without any addition of B_4C (AC0) was produced for comparison.

Ti, Mo, Nb, Al and Si were used in their elemental forms (99% purity), and B_4C was acquired as powder (98% purity, < 10μm). Ingots were prepared by vacuum arc remelting (VAR) with non-consumable tungsten electrode in a water-cooled copper crucible, achieving temperatures higher than the melting point of B_4C, which is essential for complete reaction between titanium and B_4C, according to reaction 1. To ensure better homogeneity, the melting process was repeated at least five times, turning the ingots upside down each time.

Samples were cut from the ingots and prepared following standard metallographic procedures. X-ray diffraction (XRD) was carried out for phase analysis on a Panalytical X'Pert diffractometer with Cu-Kα (λ= 0.15406 nm) at 40kV and 30mA. Phase volume and lattice parameters of the present phases were determined by Rietveld refinement of the XRD patterns on GSAS II

software. Beta phase with bcc structure (a= 0.3283 nm; space group Im-3m) was indexed with ICSD 76165 database; TiB with orthorhombic B27 structure (a = 0.612 nm, b = 0.306 nm, c = 0.456 nm; space group Pnma) was indexed with ICSD 24701 database; and TiC with B1 fcc structure (a = 0.4328 nm; space group Fm-3m) was indexed with ICSD 1546 database. Substoichiometric TiC_x particles might be formed when carbon concentration is low, however, the crystalline structure remains the same for all values of x up to 1 [25].

Scanning electron microscopy (SEM) images, for microstructural analysis, were acquired on a FEI Quanta 650 FEG, while a ZEISS Auriga Compact was employed for electron backscatter diffraction (EBSD) images, and energy dispersive X-ray spectroscopy (EDS) for composition analysis. The study of the orientation relationship between phases, as well as measurement of grains size was accomplished using Channel 5 software.

DTA curves were obtained on a NETZSCH DSC 404 F3 Pegasus in a graphite furnace cooled with chilled water with a W/Re thermocouple. Bulk samples of the composite materials weighting 90 ±5 mg were analyzed on crucibles of alumina, being subjected to a heating rate of 50°C/min, reaching a final temperature of 1700°C. Cooling at 50°C/min and 30°C/min were chosen to improve resolution of the peaks related to the formation of each phase. A continuous dynamic flow of 150 ml/min of high purity argon as purging gas was applied throughout the experiment, maintaining an inert atmosphere inside the furnace.

Nanoindentation allowed the measurement of hardness and Young's modulus of each phase, being carried out on a MTS G200 Nanoindenter equipped with a Berkovich diamond tip. Calibration on a fused silica pattern was done before measurements. The chosen technique was the continuous stiffness measurement (CSM), which allows the continuous acquisition of values of hardness and Young's modulus as a function of the depth of penetration of the indenter [26]. In this research, the maximum penetration depth was limited to 1000 nm. This method is particularly important for measurement of the properties of the beta Ti matrix. Even though large particles of TiB or TiC were avoided, minor hard particles underneath the surface, when hit by the indenter, cause significant variations on the results. An optical microscope coupled with the nanoindentation equipment allowed to pinpoint the exact position of each

indentation, with 30 impressions in each sample for determining beta phase properties, and 20 indentations in coarse TiB and TiC particle in AC3. Poisson's ratios of 0.428 for the beta phase [27], 0.160 for TiB [28] and 0.180 for TiC [29] were considered for the following expression in the calculation of Young's modulus (E_s) [26]:

$$\frac{1}{E_r} = \frac{1 - v_i^2}{E_i} + \frac{1 - v_s^2}{E_s} \qquad (2)$$

where the reduced modulus indicated by the equipment is E_r, v_s is the Poisson's ratio of the considered phase, and the indenter modulus and Poisson's ratio are characterized by E_i and v_i, having values of 1141 GPa and 0.07, respectively.

Vickers microhardness was measured for several loads from 9.8×10^{-3} N to 19.6 N using a Shimadzu tester HMV-FA2. Vickers macrohardness was measured for loads from 49 N to 294.2 N on a Centaur hardness tester (HD9-45), and indentations marks were measured on an optical microscope (Nikon Eclipse LV100). These measurements were carried out during ten seconds in ten different regions of the samples.

3. Results and discussion

3.1. Lattice parameter and microstructural analysis

Fig. 1a shows the XRD patterns of the cast materials, it can be verified that the high temperature of the VAR processing was sufficient for complete reaction between the boron carbide and the titanium alloy. This can be confirmed by the inexistence of peaks related to boron carbide or sub products such as TiB_2, while peaks matching TiB and TiC patterns can be found in the composite samples. The cooling rate inside the furnace was fast enough to avoid transformation of the beta metastable titanium phase to alpha, since there are not peaks of alpha in all samples investigated. The intensification of TiB and TiC peaks from AC0.5 to AC3 reflects the increase in volume fraction of these phases, which can also be seen in Fig. 1b, where a segment of 2θ from 35° to 43°is shown. The effect of boron carbide addition to the displacement of the most intense peak of beta phase (110) is quite noticeable, which certainly affects the value of the lattice parameter of this phase.

The results from Rietveld refinement are presented in table 1, which includes the volume and lattice parameter of each phase for each composition, and the profile parameters of the refinement, showing that the values acquired are highly reliable. According to McCusker [30], R_{wp} represents the weighted-profile residual value which should be close to R_{exp}, the statistically expected value of R. The ratio between these two parameters is the goodness-of-fit (χ^2), which should approach 1. The simple residual values are represented by R_p.

SEM images of the microstructure of AC0.5, AC1.5 and AC3 with two different magnifications are shown in Fig 2. It is clear the homogeneous distribution and increase in volume of reinforcements around the beta matrix and the results are in accordance to Rietveld refinement, being the total volume of reinforcement 4.8%, 10.6%, and 20.7% for AC0.5, AC1.5 and AC3, respectively. For AC0.5, in Fig. 2a, a dendritic distribution of the precipitates on the matrix can be easily recognized, and in Fig. 2b, most of these dark particles have the particular whisker shape of TiB, surrounded by a gray matrix of beta titanium. The brighter gray spots in the beta matrix may be regions with segregated heavier elements such as Mo and Nb, which can occur in Ti alloy produced by VAR [31,32]. In Fig 2c, there is no evidence of dendritic formation and the particles are larger than the sample with smaller composition, but without indication of primary coarse particles. The microstructure shown in Figure 2e and 2f has coarse primary phases surrounded by minor phases, possibly indicating the formation of eutectic microconstituents.

The lattice parameter of the body centered cubic phase of Ti is affected by the amount of alloying elements. The Mo element has been demonstrated to reduce the lattice parameter of beta titanium [33,34], as well as Al. While, Nb has the opposite effect, increasing cell parameter due to its higher atomic radius. From Table 1, the value of 0.3266 nm of the beta Ti in AC0 agrees with other studies with Ti-15Mo alloys [35] and Beta 21S [36].

According to phase diagram of Ti-B [23] the solubility of B in Ti is negligible, while Yan [37] demonstrated that C has solubility as low as 0.006 wt.% in Ti-15Mo alloys, so these elements have no influence on the cell parameter of beta phase. Modification of lattice parameter of the

beta phase are mainly affected by compositional variations after addition of B_4C and consequent formation of TiB and TiC, as confirmed by EDS analysis.

Table 2 shows for each sample, the composition of beta, TiB, and TiC. Due to limitations of the equipment in providing precise values of B and C elements, the results should be considered in a quantitative way. The reason for the compositional change is related to the consumption of the Ti during B_4C decomposition in TiC and TiB according to reaction 1, resulting in less titanium available for making solid solution with the remaining alloying elements. Thus, there is a reduction in the lattice parameter of beta phase to 0.3261 nm in AC0.5, 0.3259 nm in AC1.5, and 0.3255 nm in AC3.

The volume of the orthorhombic structure of the TiB increase when B composition goes from hypoeutectic to hypereutectic. The concentration of Mo and Nb increases in the TiB whisker as it coarsens, while Al is expelled from coarser borides. Boron composition increases with formation of primary TiB in AC3, while Ti concentration decreases.

TiC particles exhibit an increase in their face centered cubic unit cell with addition of B_4C, going from 0.4293 nm for AC0.5 to 0.4303 for AC3. From AC0.5 to AC3, carbon and titanium concentrations increase in the carbides, while there is a decrease in weight percentage of all remaining elements, from a total of 14.4% to 4.7% in AC0.5 and AC3, respectively. Several works have shown the relation between lattice parameters of TiC_x particles in non-stoichiometric compositions, where the cell parameter is expected to increase when approaching stoichiometry [25,38-40]. Highly substoichiometric carbides as the ones in AC0.5 have many vacancies on carbon sites, leaving spaces to be occupied by other elements, resulting in lattice parameter decrease.

3.2. Sequence of phase formation

In order to understand the effects of the composites on the formation and evolution of the microstructure, thermal analyzes were performed. The solidification process and the sequence of nucleation and growth of the precipitates explain the large quantity of substitutional atoms in the precipitates. Fig. 3 shows DTA scans for the heating process of the composite materials

up to the melting point followed by cooling. At the DTA experiments, two cooling and heating rates were used in order to enhance the quality of the analyzes. The use of high rates improves the intensity of the peaks and lowers the resolution of the signal. In AC0.5, according to Ti-B_4C isopleth [22], a solid-state mechanism takes place in eutectic TiC precipitation. Thus, atoms with higher diffusional mobility, such as Mo and Al, get faster than Ti from the beta phase to the growing TiC precipitates, explaining the high concentration of these elements and consequentially, smaller lattice parameter. Some carbides in AC1.5 also form after complete solidification of the ingot. However, when nucleate in higher temperatures, allowing better mobility of the Ti atoms. Primary TiC in AC3 nucleates and growths before beta phase formation, having enough time to consume Ti from the melt, approaching a composition closer to stoichiometry and thus larger lattice parameters. DTA curves shows that the melting of eutectic TiC start at 1541°C for AC0.5, 1539°C for AC1.5 and 1526°C for AC3, while solidification begins around 1520°C, 1530°C and 1588°C for AC0.5, AC1.5, and AC3, respectively. Primary TiC particles in the composite with larger composition of B_4C melt at 1632°C and solidify at 1692°C.

Eutectic TiB melts subsequently, being represented on the heating DTA curves at 1554°C, 1572°C and 1541°C, and solidifying at 1545°C, 1530°C and 1588°C for AC0.5, AC1.5, and AC3, respectively. Primary TiB on AC3 melts at 1654°C and solidifies at 1692°C. Eutectic beta phase melts at temperatures considerably higher than the other eutectic phases, which may be due to the larger volume of this phase causing degrees of thermal differences within the sample. For AC0.5, melting occurs at 1617°C, falling to 1607°C for AC1.5 and finally 1594°C for AC3. Solidification starts at 1565°C, 1555°C, and 1588°C for AC0.5, AC1.5 and AC3, respectively. Primary beta titanium, which is found in AC0.5 and AC1.5, is the last phase to become liquid, at 1667°C for AC0.5 and 1630°C for AC1.5, with corresponding solidification at 1692°C and 1691°C, for AC0.5 and AC1.5, respectively. It can be noticed that for AC1.5 and AC3, the cooling rate of 30°C/min was still too fast, avoiding a clear distinction between the peaks of solidification of the eutectic phases, and the primary TiB and TiC in AC3. The work of Lu [41] shows DSC curves for an alpha Ti alloy with addition of 2.6 B_4C, wt.%, having similar peaks distribution as AC1.5, however, at temperatures on average 100°C lower, which might be due to the smaller amount of alloying elements, and slower heating and cooling rates.

3.3. Crystallographic orientation relationship

Figs. 4, 5 and 6 show the EBSD analysis of as-cast titanium composites. In the central image the phases are represented in different colors, having TiB in blue, TiC in yellow and the beta matrix in black, while red lines are the beta grain boundaries. The images on the upper left corner of the Fig. 4-6 show the deviation angle from the proposed orientation relationship (OR) between TiB precipitates and beta phase in the selected region, while the respective pole figures for the indicated family of crystallographic plans are shown in the right portion of these figures. The images on the lower central region show the OR between TiC particles and beta phase. Pole figures of the OR between TiB and TiC are presented for AC0.5 and AC1.5

The coarsening of the TiB whiskers can be noticed from AC0.5 to AC3, as well as the formation of large primary TiB in the sample with the largest amount of B_4C. The deviation between TiB and beta from the orientation relationship $\{312\}_{TiB}//\{112\}_{\beta}$ seems to be large for small eutectic particles while coarse precipitates such as those present in AC3 have complete orientation. In AC0.5, TiB particles are found both inside of the beta grains and on their boundaries, but their OR is distributed over a large range of deviation angles, up to 19°. The interplanar spacing of the phases were calculated using the lattice parameters from Table 1. The difference is only 1.6% for the selected planes. Possibly, there is another factor impacting the lack of OR. A hypothesis may be related to eutectic TiB precipitates formed from the liquid, after the primary beta solidification, together with eutectic beta phase. The rapid rate of solidification imposed may have impaired the development of a proper orientation between these phases.

Studies conducted by Bilous [42] showed that in the quaternary phase diagram of Ti-Al-V-B there is a small temperature range between the eutectic temperature and complete solidification where there is coexistence of liquid with beta and TiB primary phases. This solidification sequence may explain the existence of longer whiskers in AC1.5, which are those that nucleated first, having a degree of deviation smaller than the finer eutectic particles that nucleated afterwards. In AC3, the same trend is verified. Primary TiB precipitates, which solidified first from the melt and later behave as heterogeneous nucleation sites for beta phase, show the lowest degrees of deviation, as confirmed by the specific pole figure of primary

phases. Eutectic TiB particles, on the other hand, does not verify the proposed relationship. Thence, the eutectic TiB nucleation may have occurred sympathetically on pre-existing TiB phases or rapidly along with other eutectic phases.

In Fig. 4, TiC particles do not have the typical near equiaxed shape and they seem to agglomerate near the borides, since none of them can be found far from TiB whiskers. In Fig. 5, the image of AC1.5 shows that larger TiC particles still do not have an equiaxial shape, however, in this case, the carbides are not necessarily on the surrounding of TiB whiskers. Finally, in Fig. 6, TiC particles in AC3 are composed of coarse primary and eutectic phases having a near equiaxial morphology. The carbides are located preferentially on grain boundaries and not attached to TiB particles. The relationship between TiC particles and beta changes from $\{112\}_{TiC}//\{112\}_{\beta}$ in AC0.5 to $\{113\}_{TiC}//\{112\}_{\beta}$ in AC1.5 and AC3, which has already been identified by Sarkar [43]. This seems to be explained by the sequence of solidification and nucleation, as in AC0.5, TiC nucleation involves a solid-state transformation, which justifies the fact that all TiC particles are attached or extremely close to TiB whiskers. Consequently, in AC0.5, the carbides nucleate from the borides through the following OR $\{010\}_{TiB}//\{011\}_{TiC}$, being corroborated by the difference of 0.8% between their respective interplanar spacing.

In the case of the composite AC1.5, the larger amount of C allowed the formation of coarser eutectic particles, which in this case, seem to nucleate preferentially on the beta grain boundary and also near TiB whiskers. In these samples, there is a mixture of eutectic TiC particles that nucleated straight from the melt and particles that nucleates after complete solidification of the material. The particles that nucleated on the TiB whiskers also share the same OR as the ones in AC0.5, that is, $\{010\}_{TiB}//\{011\}_{TiC}$. In AC3, coarse TiC particles clearly nucleated before the beta phase, as they are located mostly on the grain boundaries and this may justify the slight increase in deviation from the $\{113\}_{TiC}//\{112\}_{\beta}$, as in this composition, there is a competition between TiB and TiC acting as heterogeneous nucleation site for the eutectic beta phase. Pole figures for $\{010\}_{TiB}$ and $\{011\}_{TiC}$ are not shown because the number of interfaces between these phases is too small to be relevant.

3.4. Grain refinement

EBSD imaging allowed the verification of the grain size as presented in Fig 7. Near equiaxial grains of the sample AC0 are shown in Fig. 7a, while Fig. 7(b-c) show a gradual reduction in grains size to AC0.5 and AC1.5. Due to the effect of the eutectic reinforcements precipitates, restraining grain growth of primary beta grains during cooling after the melting process, and the microstructure become serrated. The change in scale reflects the great reduction in beta grain size in AC3, when primary TiB and TiC are present. The carbides and borides act as heterogeneous nucleation sites for beta precipitation when this phase is solidifying from the liquid state.

The addition of 0.5% of B_4C reduces in half the average grains size, from 504 μm for AC0 to 254 μm for AC0.5, while for AC1.5 there is a reduction to 192 μm. Grains in AC3 present a considerable reduction in size, becoming ten times smaller than the previous composition, reaching 18 μm on average. The reduction in grain size from AC0 to AC0.5 may be attributed to constitutional supercooling, which also explains dendritic formation. In this case, due to extremely low solubility of boron in titanium, when beta grains are nucleating and growing, boron is expelled to the solid-liquid interface. The segregated boron then forms TiB whiskers, acting as pinning particles avoiding posterior grain growth [44]. The irregular shape of the grains is a sign of this restraining effect imposed mostly by TiB whiskers. In AC1.5, where beta, TiB and TiC phases nucleate and grow at similar time, the previous phenomenon that leads to dendritic formation is not evident, but the pinning effect is more pronounced due to larger amount of precipitates. In AC3, the reduction effect is primarily caused by TiB and TiC coarse precipitates that are formed previously than the beta phase. Due to the high cooling rates imposed by the VAR process and the substantial excess of C and B, the number of TiC and TiB precipitates is higher. Therefore, the number of nucleation sites of the beta phase is increased. Consequently, from the nucleation and growth mechanisms and also due the orientation relationships established through the EBSD, when compared to the other compositions, it exhibits elevated microstructural refinement.

3.5. Mechanical Properties

Fig. 8 presents an evaluation of hardness and Young's modulus from nanoindentation for a continuous range of loads applied on beta phase, on TiB and TiC coarse particles. The dependence of hardness of the materials were also evaluated by Vickers microhardness and macrohardness.

Young's modulus of the beta phase increases when addition of B_4C also increase. The nanoindentation was carried out in regions as far as possible from particles visible on the surface, and curves with abnormal increase in values underneath the surface were discarded. However, the effect of small eutectic precipitates should be considered. Strengthening by solid solution might also affect modulus, as Al has been demonstrated to increase elastic modulus [45]. Zhang and co-workers [46] investigated the effect of Mo on Ti-Mo alloys and concluded that from 15 wt.% Mo the modulus of elasticity increases proportionally with the increase of the alloying elements. The phenomenon of indentation size effect, where modulus decreases as indentation load increases [47] is evident for AC0, which can be considered a single crystal due to large grain size and where grain boundaries do not influence dislocation movement. This phenomenon however, is not seen in AC0.5, AC1.5 and AC3, because the homogenous distribution of precipitates act as barriers for geometrical necessary dislocations movement.

Hardness increases with B_4C addition and values acquired by nanoindentation at 70mN drop 30 to 40% when measurement procedure is modified to Vickers microhardness for 98mN. Similar reduction of hardness values from one method to another has been verified by other researches [48,49]. The type of instrument seems to affect results, as seen in the transition from micro to macrohardness, where values decrease for the smallest load in the macrohardness tester. Indentation of bcc materials have been demonstrated to follow a typical hardness-displacement behavior [50], where three regions are usually seen, starting with a decrease in hardness, followed by an increase due to local hardening, and lastly a softening for higher loads or depths of indentation penetration.

The curves of hardness presented in Fig. 8 seem to follow this proposed characteristic. Nevertheless, the reason is not as straightforward as for alloys or pure materials, because reinforcements in composites add several factors that should be taken into consideration. Solid

solution of B and C is not considered a strengthening mechanism in the materials developed due to negligible solubility of both elements, however, the increase in composition of alloying elements in solid solution in beta phase, as it is from AC0 to AC3 increases hardness [51].

For nanohardness, grain size does not influence on values since grains are much larger than indentations, however, for micro and macrohardness measurements, the strengthening effect due to smaller grain size must be accounted since indentation diagonal sizes reach values around 400 μm for the largest loads. The reduction in grain size seen in composites is a factor that reduces mobility of dislocations generated during indentation. The change of deformation mode from slip to stress-induced phase formation such as ω or martensitic α (α") in Ti-Mo alloys has been investigated in several works [52-54] and this mechanism could also play a role in strain hardening as indentation is carried out. The formation of in-situ carbides creates tensions around the particles due to difference in coefficient of thermal expansion (CTE) between Ti in Beta 21S (8.5×10^{-6} K^{-1}) [55] and TiC (7.4×10^{-6} K^{-1}) [56] altering hardness, especially when large primary TiC particles are present, as the case of AC3. CTE of TiB (8.6×10^{-6} K^{-1}) [57] is closer to Ti affecting hardness on a smaller degree. For higher loads it is impossible to avoid striking particles, and the distinction between values of hardness for the materials as a matrix plus reinforcements, not only beta phase, becomes clearer. It can be identified from Fig. 8 that the starting point for considering the hardness of the materials as composites, and not only as a single grain of beta phase, is at 1000 mN, where the values of all composites increase considerably, while AC0 remains constant. Values of microhardness on loads higher than 1000 mN seem to reach the highest values between 2 and 5N, decreasing for higher loads up to 50 N. On macrohardness measurements, hardness increases to highest values between 100 and 200N, decreasing afterwards.

Nanoindentation was also used to measure hardness and elastic modulus of primary TiB and TiC particles in AC3, and the already mentioned indentation size effect is clear for both properties. Initial values of modulus reach 550 GPa for TiB and 350 GPa for TiC, and hardness of 32.5 GPa and 25 GPa for TiB and TiC, respectively. Different methods have been used by many other authors to determine Young's modulus, ranging from 200 GPa to 750 GPa for TiB [28,58-

59] and 410 GPa to 510 GPa for TiC [56], where the higher values for TiC might be related to the stoichiometry of the carbides. Hardness has been reported to be around 27.5 GPa [60] for TiB, which is within the range of nanoindentation values found in the current work, and 28 to 35 GPa for TiC [56], which again are higher because these researchers may have used TiC closer to stoichiometric values.

4. Conclusions

Adding B_4C to the Beta 21S alloy on as-cast condition causes variation of lattice parameters in beta phase because Ti is consumed during formation of in-situ TiB and TiC, and other alloying elements become more abundant in solid solution. Increasing amount of Mo may be the reason for lattice parameter reduction of beta Ti as B_4C amount is increased. Total volume of the crystalline cell of TiB precipitates increases from hypoeutectic composition of boron in AC0.5 to a hypereutectic in AC3, where primary precipitates are formed. Mo and Nb concentration increases in coarse precipitates while Al is expelled from them. TiC particles in AC0.5 are highly substoichiometric, containing large amounts of substitutional elements, while increasing C concentration causes the formation of primary particles in AC3, with larger lattice parameters and higher concentration of Ti and C, that is, closer to stoichiometry.

The sequence of formation of phases from the melt was determined to be the following:

- AC0.5: $L \rightarrow L + Beta_p \rightarrow Beta_p + (Beta + TiB)_{eut} \rightarrow Beta_p + (Beta + TiB + TiC)_{eut}$
- AC1.5: $L \rightarrow L + Beta_p \rightarrow Beta_p + (Beta + TiB + TiC)_{eut}$
- AC3: $L \rightarrow L + (TiB + TiC)_p \rightarrow (TiB + TiC)_p + (Beta + TiB + TiC)_{eut}$

Specific crystallographic orientation relationship between beta and TiB were determined to be $\{312\}_{TiB}$// $\{112\}_{Beta}$, where large TiB whiskers have the smallest deviation degree. OR between beta and TiC changed from $\{112\}_{TiC}$// $\{112\}_{Beta}$ in AC0.5 to $\{113\}_{TiC}$ // $\{112\}_{Beta}$ in AC1.5 and AC3, and TiC particles nucleated from TiB in AC0.5 and AC1.5 according to $\{010\}_{TiB}$//$\{011\}_{TiC}$.

Grain size reduced to half with addition of 0.5 B_4C, wt.%, from 504 µm to 254 µm, and higher reductions were only achieved when primary precipitates where formed, acting as

heterogeneous nucleation site for beta nucleation, as the case of AC3, with beta grain size of 18 μm.

Compositional variation, grain refinement, and in-situ particles precipitation can affect mechanical properties. Nanoindentation showed that Young's modulus of beta increases as B_4C composition increases, from 87 GPa for AC0 to 130 GPa for AC3, while hardness shows similar trend, with initial values of 4.6 GPa and 6.2GPa for AC0 and AC3, respectively. Modulus and hardness of coarse TiB and TiC particles were measured as well. Micro and macro hardness tests were employed to verify that at 1000 mN, hardness measurements changed from single phase to multiphase, where the formation of in-situ precipitates modifies the mechanical properties on larger scales.

Acknowledgement

The authors gratefully acknowledge the Brazilian research funding agencies CNPq (National Council for Scientific and Technological Development) and CAPES (Federal Agency for the Support and Evaluation of Graduate Education) for their partial financial support of this work. The authors also gratefully acknowledge the use of experimental facilities at Brazilian Nanotechnology National Laboratory (LNNano), the Electron Microscopy Service and Materials Technology Institute at the Polytechnic University of Valencia.

References

[1] Panda, K. B., and KS Ravi Chandran. "Synthesis of ductile titanium-titanium boride (Ti-TiB) composites with a beta-titanium matrix: The nature of TiB formation and composite properties." *Metallurgical and materials transactions A* 34.6 (2003): 1371-1385. https://doi.org/10.1007/s11661-003-0249-z

[2] He, Guo, et al. "Novel Ti-base nanostructure–dendrite composite with enhanced plasticity." *Nature materials* 2.1 (2003): 33. https://doi.org/10.1038/nmat792

[3] Okulov, Ilya V., et al. "High strength beta titanium alloys: New design approach." *Materials Science and Engineering: A* 628 (2015): 297-302. https://doi.org/10.1016/j.msea.2015.01.073

[4] Rahoma, H. K. S., et al. "Influence of (TiC+ TiB) on the microstructure and tensile properties of Ti-B20 matrix alloy." *Journal of Alloys and Compounds* 627 (2015): 415-422. https://doi.org/10.1016/j.jallcom.2014.12.056

[5] Fanning, J. C., and S. P. Fox. "Recent developments in metastable β strip alloys." *Journal of materials engineering and performance* 14.6 (2005): 703-708. https://doi.org/10.1361/105994905X75484

[6] Ivasishin, O. M., et al. "A comparative study of the mechanical properties of high-strength β-titanium alloys." *Journal of alloys and compounds* 457.1-2 (2008): 296-309. https://doi.org/10.1016/j.jallcom.2007.03.070

[7] Cotton, James D., et al. "State of the art in beta titanium alloys for airframe applications." *Jom* 67.6 (2015): 1281-1303. https://doi.org/10.1007/s11837-015-1442-4

[8] Weiss, I., and S. L. Semiatin. "Thermomechanical processing of beta titanium alloys—an overview." *Materials Science and Engineering: A* 243.1-2 (1998): 46-65. https://doi.org/10.1016/S0921-5093(97)00783-1

[9] Sun, Shuyu, et al. "The influences of trace TiB and TiC on microstructure refinement and mechanical properties of in situ synthesized Ti matrix composite." *Composites Part B: Engineering* 43.8 (2012): 3334-3337. https://doi.org/10.1016/j.compositesb.2012.01.075

[10] Tamirisakandala, S., et al. "Grain refinement of cast titanium alloys via trace boron addition." *Scripta Materialia* 53.12 (2005): 1421-1426. https://doi.org/10.1016/j.scriptamat.2005.08.020

[11] Cherukuri, Balakrishna, et al. "The influence of trace boron addition on grain growth kinetics of the beta phase in the beta titanium alloy Ti–15Mo–2.6 Nb–3Al–0.2 Si." *Scripta Materialia* 60.7 (2009): 496-499. https://doi.org/10.1016/j.scriptamat.2008.11.040

[12] Cai, Lifang, et al. "Research on development of in situ titanium matrix composites and in situ reaction thermodynamics of the reaction systems." *Journal of University of Science and Technology Beijing, Mineral, Metallurgy, Material* 13.6 (2006): 551-557. https://doi.org/10.1016/S1005-8850(06)60112-6

[13]Ho, W. F., C. P. Ju, and JH Chern Lin. "Structure and properties of cast binary Ti–Mo alloys." Biomaterials 20.22 (1999): 2115-2122. https://doi.org/10.1016/S0142-9612(99)00114-3

[14]Oliveira, Nilson TC, et al. "Development of Ti–Mo alloys for biomedical applications: microstructure and electrochemical characterization." Materials Science and Engineering: A 452 (2007): 727-731. https://doi.org/10.1016/j.msea.2006.11.061

[15]Morsi, K., and V. V. Patel. "Processing and properties of titanium–titanium boride (TiBw) matrix composites—a review." *Journal of materials science* 42.6 (2007): 2037-2047. https://doi.org/10.1007/s10853-006-0776-2

[16] Zhang, Erlin, Songyan Zeng, and Bin Wang. "Preparation and microstructure of in situ particle reinforced titanium matrix alloy." *Journal of materials processing technology* 125 (2002): 103-109. https://doi.org/10.1016/S0924-0136(02)00329-1

[17] Huang, L_J, et al. "In situ TiBw/Ti–6Al–4V composites with novel reinforcement architecture fabricated by reaction hot pressing." *Scripta materialia* 60.11 (2009): 996-999. https://doi.org/10.1016/j.scriptamat.2009.02.032

[18] Zhu, J. H., et al. "High-temperature mechanical behavior of Ti-6Al-4V alloy and TiC p/Ti-6Al-4V composite." *Metallurgical and Materials Transactions A* 30.6 (1999): 1569-1578. https://doi.org/10.1007/s11661-999-0094-9

[19] Bermingham, M. J., et al. "Effects of boron on microstructure in cast titanium alloys." *Scripta Materialia* 59.5 (2008): 538-541. https://doi.org/10.1016/j.scriptamat.2008.05.002

[20]Chandravanshi, V. K., et al. "Effect of boron on microstructure and mechanical properties of thermomechanically processed near alpha titanium alloy Ti-1100." *Journal of Alloys and Compounds* 509.18 (2011): 5506-5514. https://doi.org/10.1016/j.jallcom.2011.02.114

[21]Sarkar, R., et al. "Structure–property correlation of a boron and carbon modified as cast β titanium alloy." *Philosophical Magazine* 93.15 (2013): 1936-1957. https://doi.org/10.1080/14786435.2013.765979

[22]Duschanek, H., P. Rogl, and H. L. Lukas. "A critical assessment and thermodynamic calculation of the boron-carbon-titanium (BC-Ti) ternary system." *Journal of phase equilibria* 16.1 (1995): 46-60. https://doi.org/10.1007/BF02646248

[23] Murray, J. L., P. K. Liao, and K. E. Spear. "The B− Ti (Boron-Titanium) system." *Bulletin of Alloy Phase Diagrams* 7.6 (1986): 550-555. https://doi.org/10.1007/BF02869864

[24] Okamoto, H. "C-Ti (carbon-titanium)." *Journal of Phase Equilibria and Diffusion* 19.1 (1998): 89-89. https://doi.org/10.1007/s11669-006-5014-8

[25] Pearson, William Burton. A handbook of lattice spacings and structures of metals and alloys: International series of monographs on metal physics and physical metallurgy. Vol. 4. Elsevier, 2013.

[26]Oliver, Warren Carl, and George Mathews Pharr. "An improved technique for determining hardness and elastic modulus using load and displacement sensing indentation experiments." Journal of materials research 7.6 (1992): 1564-1583. https://doi.org/10.1557/JMR.1992.1564

[27]Ikehata, Hideaki, et al. "First-principles calculations for development of low elastic modulus Ti alloys." Physical Review B 70.17 (2004): 174113. https://doi.org/10.1103/PhysRevB.70.174113

[28] Atri, R. R., K. S. Ravichandran, and S. K. Jha. "Elastic properties of in-situ processed Ti–TiB composites measured by impulse excitation of vibration." Materials Science and Engineering: A 271.1-2 (1999): 150-159. https://doi.org/10.1016/S0921-5093(99)00198-7

[29]Dodd, S. P., M. Cankurtaran, and B. James. "Ultrasonic determination of the elastic and nonlinear acoustic properties of transition-metal carbide ceramics: TiC and TaC." Journal of materials science 38.6 (2003): 1107-1115. https://doi.org/10.1023/A:1022845109930

[30]McCusker, L. B., et al. "Rietveld refinement guidelines." Journal of Applied Crystallography 32.1 (1999): 36-50. https://doi.org/10.1107/S0021889898009856

[31]Mitchell, A. "Solidification in remelting processes." Materials Science and Engineering: A 413 (2005): 10-18. https://doi.org/10.1016/j.msea.2005.08.157

[32]Banerjee, Dipankar, and J. C. Williams. "Perspectives on titanium science and technology." Acta Materialia 61.3 (2013): 844-879. https://doi.org/10.1016/j.actamat.2012.10.043

[33]Terauchi, S., et al. "Investigation of the Titanium--Molybdenum Binary Phase Diagram." Titanium and Titanium Alloys, Scientific and Technological Aspects, 2 (1976): 1335-1349.

[34] Murray, Joanne L. "The Mo− Ti (Molybdenum-Titanium) system." Bulletin of Alloy Phase Diagrams 2.2 (1981): 185-192. https://doi.org/10.1007/BF02881476

[35]Severino Martins Jr, José Roberto, and Carlos Roberto Grandini. "Structural characterization of Ti-15Mo alloy used as biomaterial by Rietveld method." Journal of Applied Physics 111.8 (2012): 083535. https://doi.org/10.1063/1.4707920

[36]Malinov, S., et al. "Synchrotron X-ray diffraction study of the phase transformations in titanium alloys." Materials Characterization 48.4 (2002): 279-295. https://doi.org/10.1016/S1044-5803(02)00286-3

[37]Yan, M., et al. "Impacts of trace carbon on the microstructure of as-sintered biomedical Ti–15Mo alloy and reassessment of the maximum carbon limit." Acta biomaterialia 10.2 (2014): 1014-1023. https://doi.org/10.1016/j.actbio.2013.10.034

[38] Holt, J. B., and Z. A. Munir. "Combustion synthesis of titanium carbide: theory and experiment." Journal of Materials Science 21.1 (1986): 251-259. https://doi.org/10.1007/BF01144729

[39] Zarrinfar, N., et al. "Carbide stoichiometry in TiCx and Cu–TiCx produced by self-propagating high-temperature synthesis." Scripta materialia 46.2 (2002): 121-126. https://doi.org/10.1016/S1359-6462(01)01205-2

[40]Lin, Y., R. H. Zee, and B. A. Chin. "In situ formation of three-dimensional TiC reinforcements in Ti-TiC composites." Metallurgical Transactions A 22.4 (1991): 859-865. https://doi.org/10.1007/BF02658995

[41] Lu, Weijie, et al. "Microstructure and tensile properties of in situ synthesized (TiBw+ TiCp)/Ti6242 composites." Journal of materials science 36.15 (2001): 3707-3714. https://doi.org/10.1023/A:1017917631855

[42] Bilous, O. O., et al. "Effect of boron on the structure and mechanical properties of Ti–6Al and Ti–6Al–4V." Materials Science and Engineering: A 402.1-2 (2005): 76-83. https://doi.org/10.1016/j.msea.2005.05.011

[43] Sarkar, Rajdeep, et al. "Crystallographic orientation relationships of boride and carbide particles with α and β phases in a β-Ti alloy." Journal of Alloys and Compounds 612 (2014): 435-442. https://doi.org/10.1016/j.jallcom.2014.05.202

[44] Tamirisakandala, S., et al. "Grain refinement of cast titanium alloys via trace boron addition." Scripta Materialia 53.12 (2005): 1421-1426. https://doi.org/10.1016/j.scriptamat.2005.08.020

[45] Collings, E. W., H. L. Gegel, and J. C. Ho. Solid solution strengthening and fundamental design of titanium alloys. No. AFML-TR-72-171. AIR FORCE MATERIALS LAB WRIGHT-PATTERSON AFB OH, 1972.

[46]Zhang, Wei-dong, et al. "Elastic modulus of phases in Ti–Mo alloys." Materials Characterization 106 (2015): 302-307. https://doi.org/10.1016/j.matchar.2015.06.008

[47] Pharr, George M., Erik G. Herbert, and Yanfei Gao. "The indentation size effect: a critical examination of experimental observations and mechanistic interpretations." Annual Review of Materials Research 40 (2010): 271-292. https://doi.org/10.1146/annurev-matsci-070909-104456

[48]Qian, Linmao, et al. "Comparison of nano-indentation hardness to microhardness." Surface and Coatings Technology 195.2-3 (2005): 264-271. https://doi.org/10.1016/j.surfcoat.2004.07.108

[49]Kim, H. H., S. H. Cho, and C. G. Kang. "Evaluation of microstructure and mechanical properties by using nano/micro-indentation and nanoscratch during aging treatment of rheo-forged Al 6061 alloy." Materials Science and Engineering: A 485.1-2 (2008): 272-281. https://doi.org/10.1016/j.msea.2007.07.085

[50] Voyiadjis, George Z., Amin H. Almasri, and Taehyo Park. "Experimental nanoindentation of BCC metals." Mechanics Research Communications 37.3 (2010): 307-314. https://doi.org/10.1016/j.mechrescom.2010.02.001

[51] Jaffee, R. I. "The physical metallurgy of titanium alloys." Progress in metal physics 7 (1958): 65-163. https://doi.org/10.1016/0502-8205(58)90004-2

[52] Kim, Han-Sol, et al. "Stress-induced martensitic transformation of metastable β-titanium alloy." Materials Science and Engineering: A 449 (2007): 322-325. https://doi.org/10.1016/j.msea.2006.02.329

[53] Hida, M., et al. "Stress induced products and ductility due to lattice instability of β phase single crystal of Ti-Mo alloys." Acta Metallurgica 30.8 (1982): 1471-1479. https://doi.org/10.1016/0001-6160(82)90167-5

[54] Wood, R. M. "Martensitic alpha and omega phases as deformation products in a titanium-15% molybdenum alloy." Acta metallurgica 11.8 (1963): 907-914. https://doi.org/10.1016/0001-6160(63)90060-9

[55] Welsch, Gerhard, Rodney Boyer, and E. W. Collings, eds. Materials properties handbook: titanium alloys. ASM international, 1993.

[56] Pierson, Hugh O. Handbook of refractory carbides and nitrides: properties, characteristics, processing and applications. William Andrew, 1996.

[57] Saito, Takashi. "The automotive application of discontinuously reinforced TiB-Ti composites." JOM 56.5 (2004): 33-36. https://doi.org/10.1007/s11837-004-0125-3

[58] Fan, Z., et al. "The Young's moduli of in situ Ti/TiB composites obtained by rapid solidification processing." Journal of materials science 29.4 (1994): 1127-1134. https://doi.org/10.1007/BF00351442

[59] Gorsse, Stéphane, et al. "Investigation of the Young's modulus of TiB needles in situ produced in titanium matrix composite." Materials Science and Engineering: A 340.1-2 (2003): 80-87. https://doi.org/10.1016/S0921-5093(02)00188-0

[60] Cao, Guojian, Lin Geng, and Masaaki Naka. "Elastic properties of titanium monoboride measured by nanoindentation." Journal of the American Ceramic Society 89.12 (2006): 3836-3838. https://doi.org/10.1111/j.1551-2916.2006.01280.x

Highlights

Title: Microstructural evolution and mechanical properties of in-situ as-cast beta titanium matrix composites

Authors: Vitor V. Rielli; Vicente Amigó-Borras; Rodrigo J. Contieri

- TiB and TiC in-situ particles are produced after melting, while varying composition;
- There is a clear orientation relationship between matrix and coarse precipitates;
- Lattice parameter of beta titanium decreases with increase in volume of TiB and TiC;
- Addition of 3% of B_4C to Beta 21S reduced grain size from 504 µm to up to 18 µm;
- Young's modulus and hardness from nano to macro increased with addition of B_4C.

Table captions

Table 1

Rietveld refinement results from the XRD patterns of as-cast Beta 21S alloy and Ti β-B_4C composites

Table 2

EDS results of spot analyses of Ti Beta matrix and TiC and TiB compounds (wt.%)

Table 1

	Phase volume (%)				Lattice Parameter (nm)					Profile Parameters			
	Beta	TiB	TiC	Total of reinforcements	Beta	TiB			TiC	R_{wp} (%)	R_{exp} (%)	R_p (%)	χ^2
					a	a	b	c	a				
AC0	100	-	-	-	0.3266	-	-	-	-	9.88	5.57	6.72	1.77
AC0.5	95.2	3.9	0.9	4.8	0.3261	0.6091	0.3043	0.4578	0.4293	8.20	5.83	6.50	1.41
AC1.5	89.4	8.1	2.5	10.6	0.3259	0.6095	0.3054	0.4564	0.4298	8.96	5.55	6.35	1.61
AC3	79.3	15.3	5.4	20.7	0.3255	0.6098	0.3055	0.4562	0.4303	9.54	5.05	6.66	1.89

Table 2

	Beta					TiB						TiC					
	Al	Nb	Mo	Si	Ti	Al	Nb	Mo	Si	Ti	B	Al	Nb	Mo	Si	Ti	C
AC0	2.9	3.2	14.9	0.3	78.7	-	-	-	-	-	-	-	-	-	-	-	-
AC0.5	3	2.9	15.5	0.4	78.2	0.9	2	6.3	0.2	53.4	37.2	2	2.4	9.6	0.4	77.5	8.1
AC1.5	3	2.8	15.9	0.4	77.9	0.4	2.3	6.4	0.1	53.5	37.3	0.8	1.3	3.7	0.6	82.9	10.7
AC3	3.2	3.3	16.6	0.2	76.7	0.1	2.6	7.5	0	49.9	39.9	0.6	1.4	2.6	0.1	83.9	11.4

Figure captions

Fig. 1. a) XRD patterns of as-cast Beta 21S and composites with in-situ synthesized TiB and TiC particles. Red lines are the experimental values, black lines are the values calculated through Rietveld refinement, and blue lines are the difference between experimental and calculated values. b) Magnified XRD pattern of the 2θ segment from 35° to 43° showing the most intense peaks of the existing phases, where intensity of TiB and TiC peaks increase with B_4C addition, and the (110)β peak changes in 2θ position

Fig. 2. Backscattered SEM images of the composite materials. (a, b) AC0.5; (c, d) AC1.5; (e, f) AC3.

Fig. *3*. DTA scan of the composite materials during heating at a rate of 50°C/min and cooling at 50°C/min and 30°C/min (dashed lines).

Fig. 4. Phase map of the AC0.5 composite, showing *in-situ* TiB (blue) and TiC (yellow) on a beta titanium matrix (black). Left upper corner: deviation degree from the $\{312\}_{TiB}$// $\{112\}_{Beta}$ between TiB and beta. Lower central image: deviation degree from the $\{112\}_{TiC}$// $\{112\}_{Beta}$ between TiC beta. Pole figures of $\{112\}_{Beta}$, $\{312\}_{TiB}$,$\{010\}_{TiB}$,$\{112\}_{TiC}$, and $\{011\}_{TiC}$ are depicted on the right portion of the figure.

Fig. 5. Phase map of the AC1.5 composite, showing *in-situ* TiB (blue) and TiC (yellow) on a beta titanium matrix (black) and grain boundaries (red lines). Left upper corner: deviation degree from the $\{312\}_{TiB}$// $\{112\}_{Beta}$ between TiB and beta. Lower central image: deviation degree from the $\{113\}_{TiC}$// $\{112\}_{Beta}$ between TiC beta. Pole figures of $\{112\}_{Beta}$, $\{312\}_{TiB}$,$\{010\}_{TiB}$,$\{113\}_{TiC}$, and $\{011\}_{TiC}$ are depicted on the right portion of the figure.

Fig. 6. Phase map of the AC3 composite, showing *in-situ* TiB (blue) and TiC (yellow) on a beta titanium matrix (black) and grain boundaries (red lines). Left upper corner: deviation degree from the $\{312\}_{TiB}$// $\{112\}_{Beta}$ between TiB and beta. Lower central image: deviation degree from the $\{113\}_{TiC}$// $\{112\}_{Beta}$ between TiC beta. Pole figures of $\{112\}_{Beta}$, $\{312\}_{TiB}$ for primary and eutectic TiB, and$\{113\}_{TiC}$ are depicted on the right portion of the figure.

Fig. 7. EBSD map showing grains size and shape of central regions of the ingots. (a) AC0; (b) AC0.5; (c) AC1.5; (d) AC3.

Fig. 8. Nanohardness (lower left corner) and Young's modulus (upper left corner) for beta phase; nanohardness and Young's modulus of TiB and TiC coarse particles from AC3 (upper right corner); Vickers micro and macrohardness of the materials (lower right corner).

Figure 1

Click here to download high resolution image

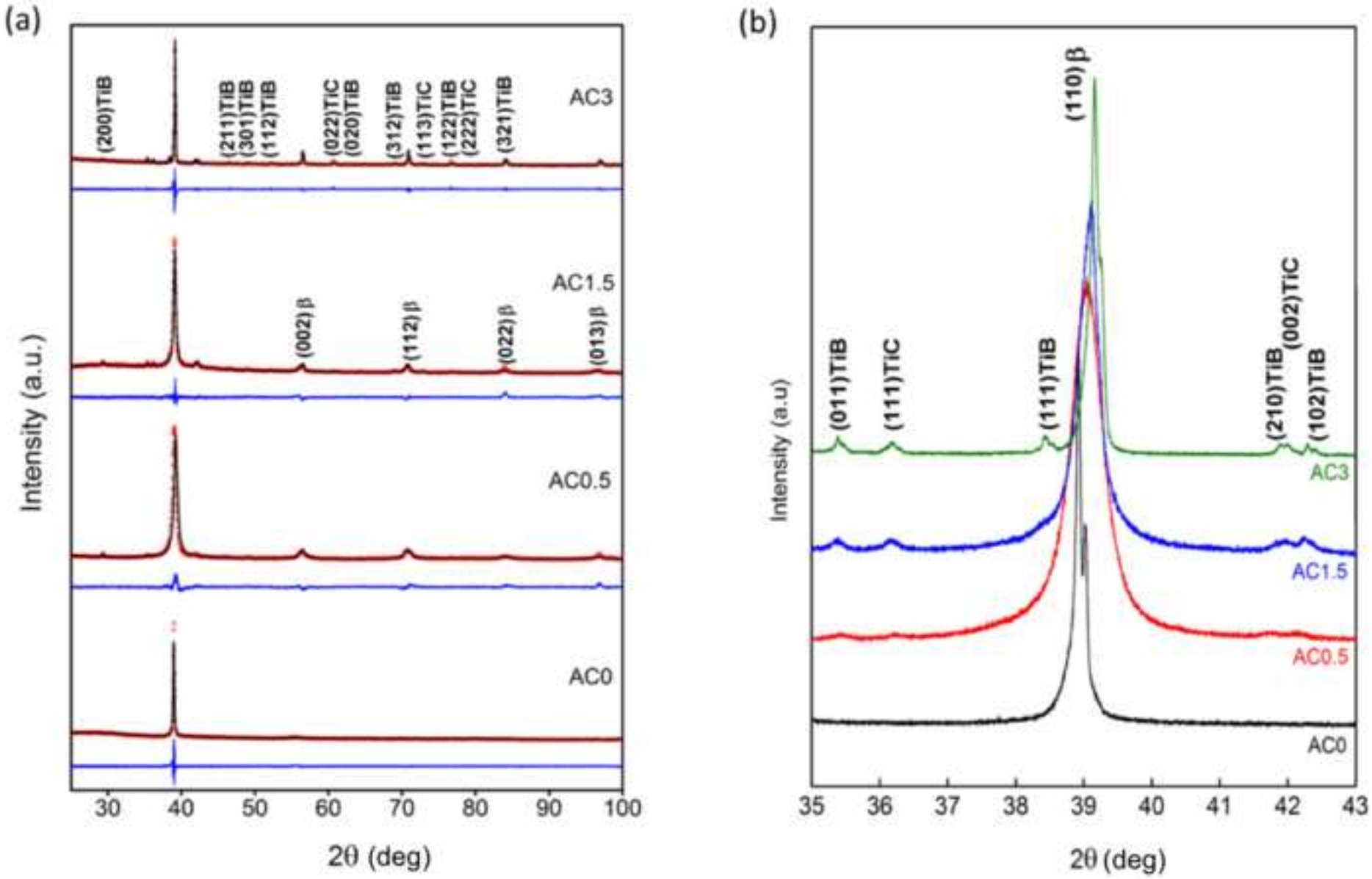

Figure 2

Click here to download high resolution image

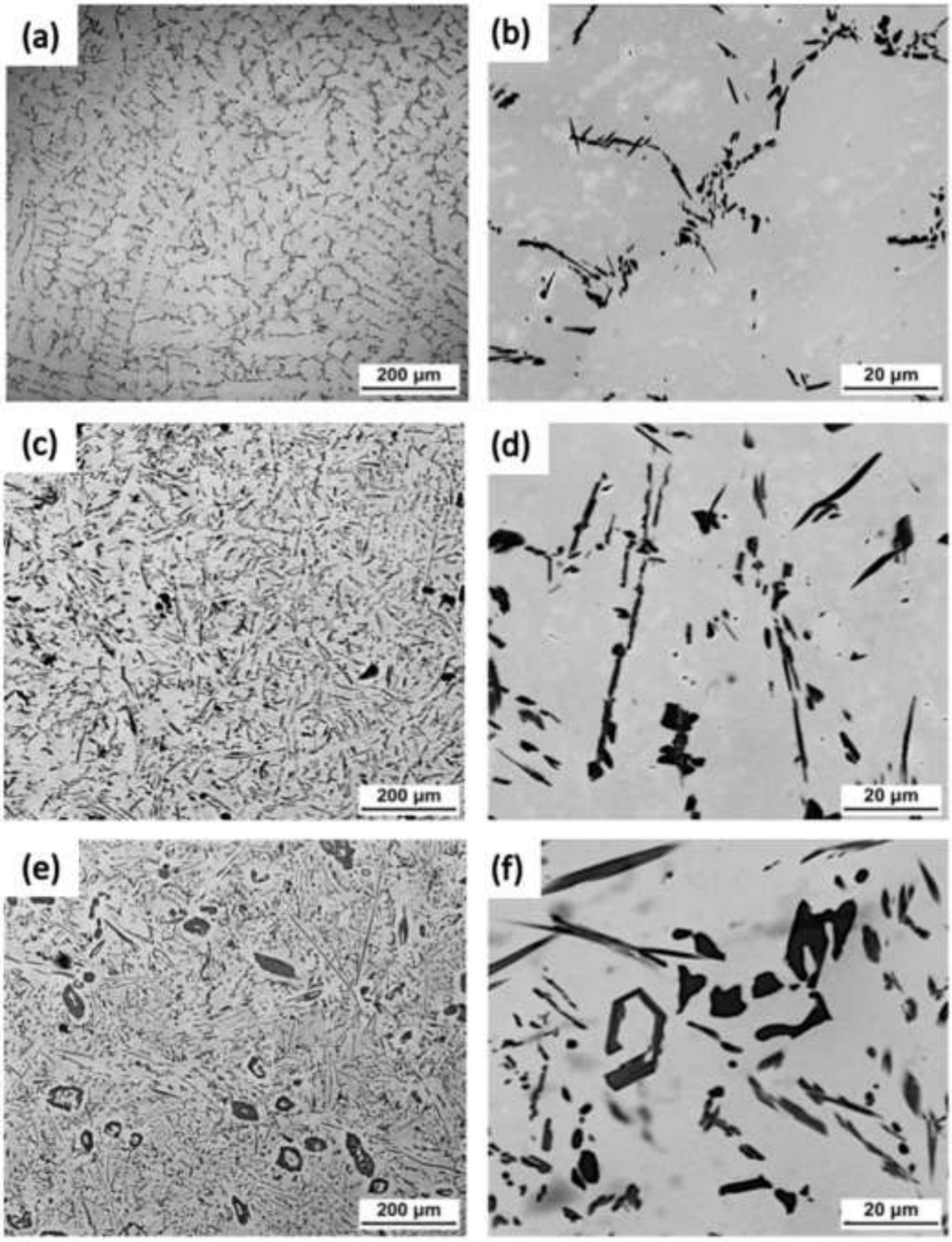

Figure 3

Click here to download high resolution image

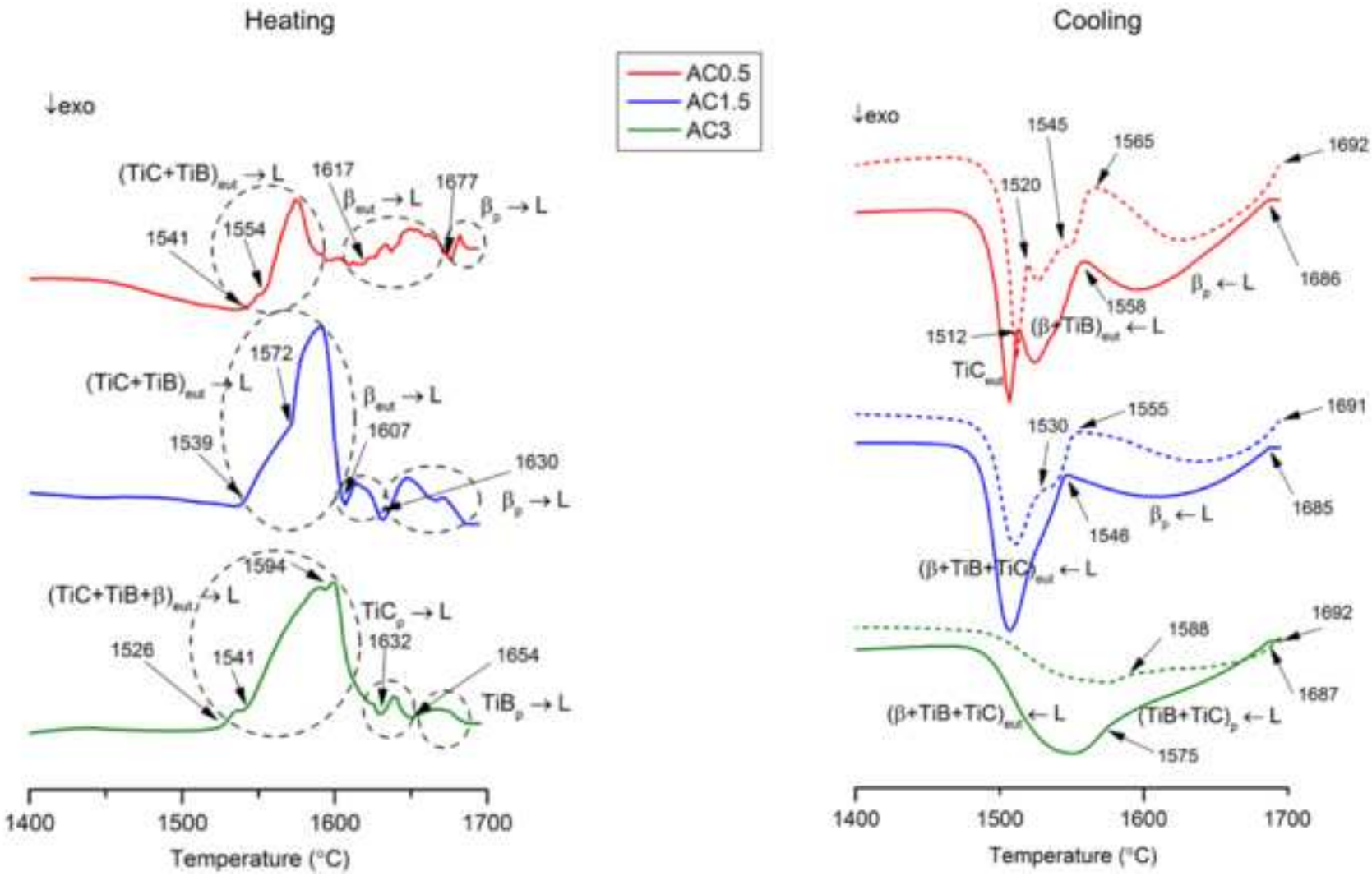

Figure 4

Click here to download high resolution image

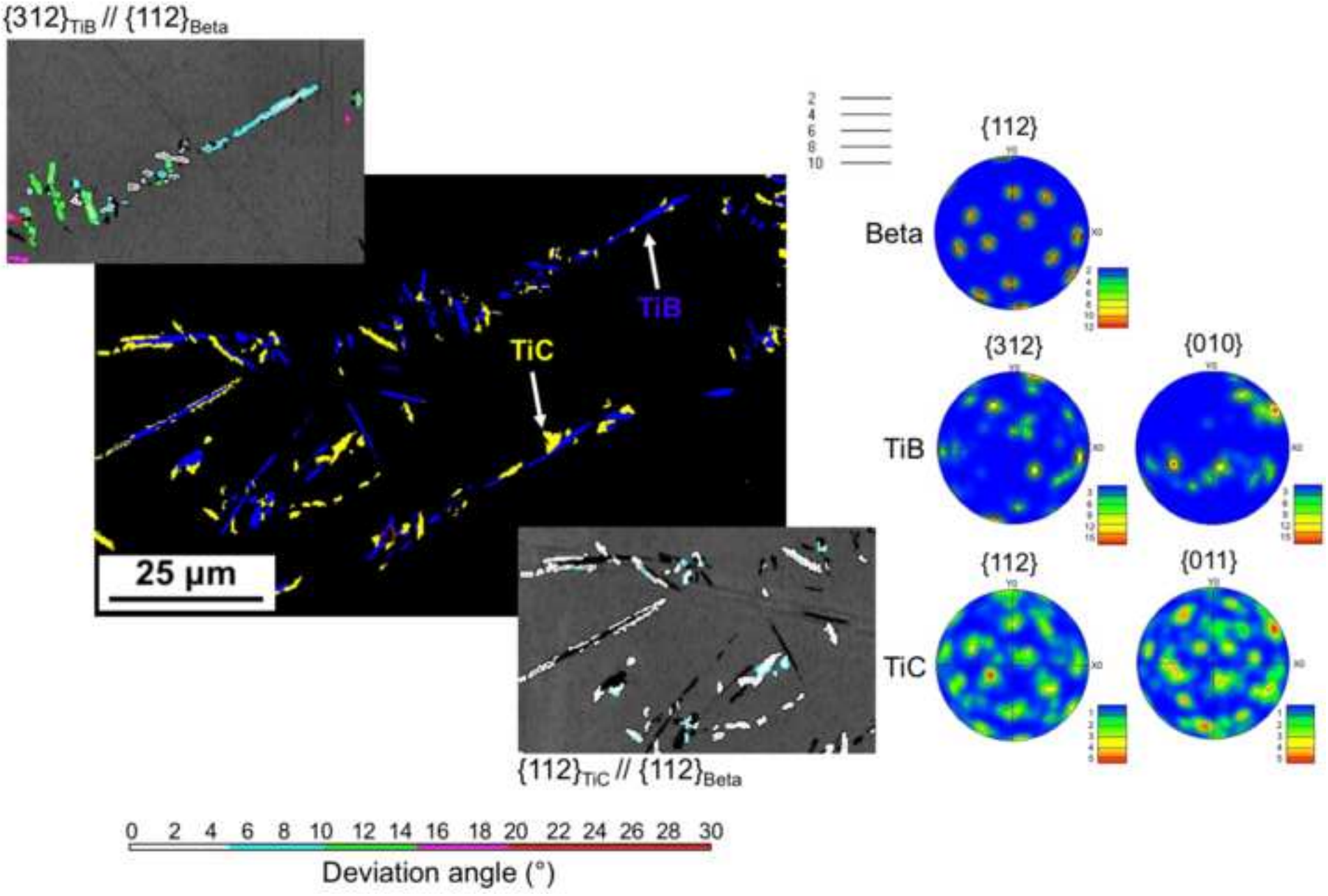

Figure 5

Click here to download high resolution image

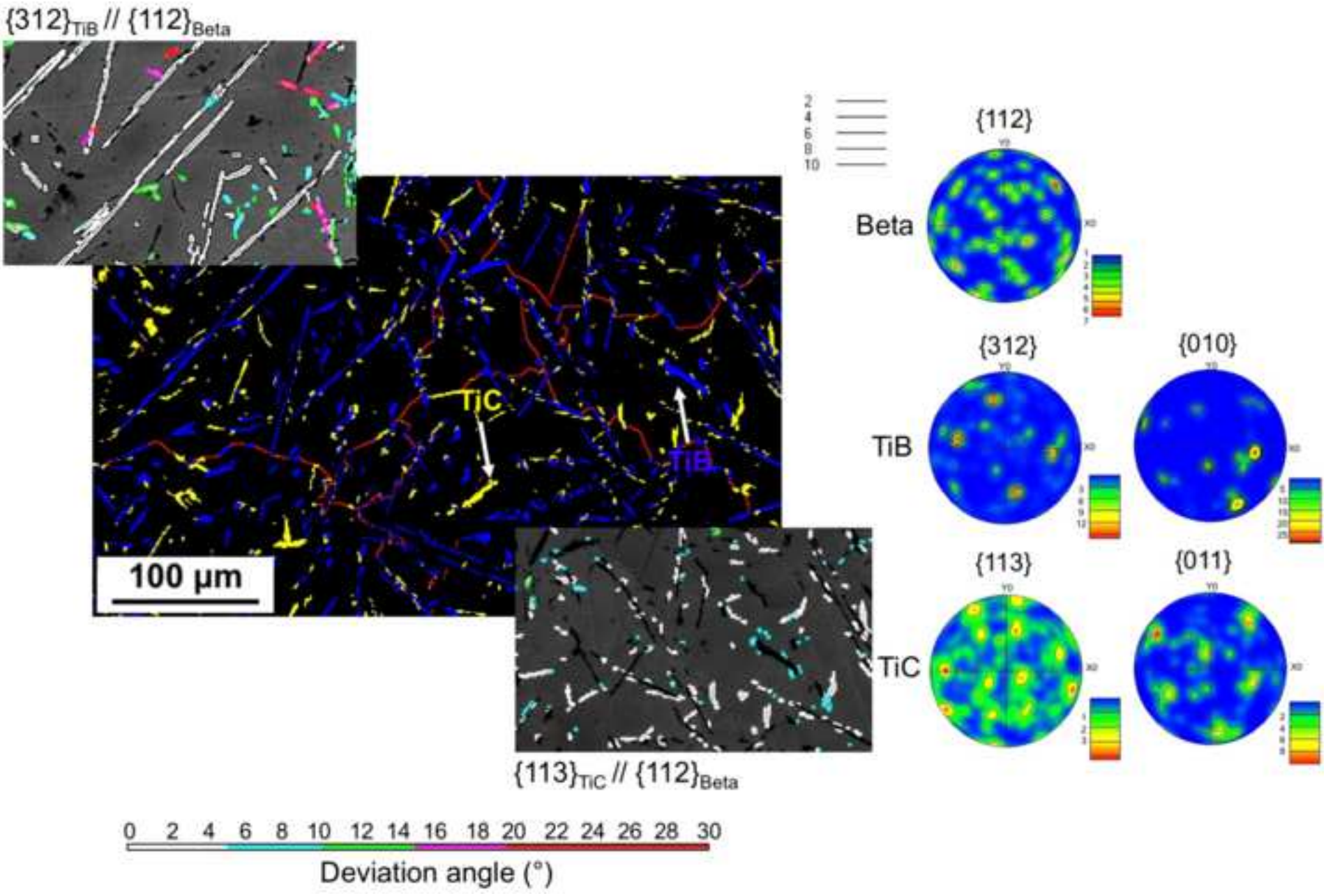

Figure 6

Click here to download high resolution image

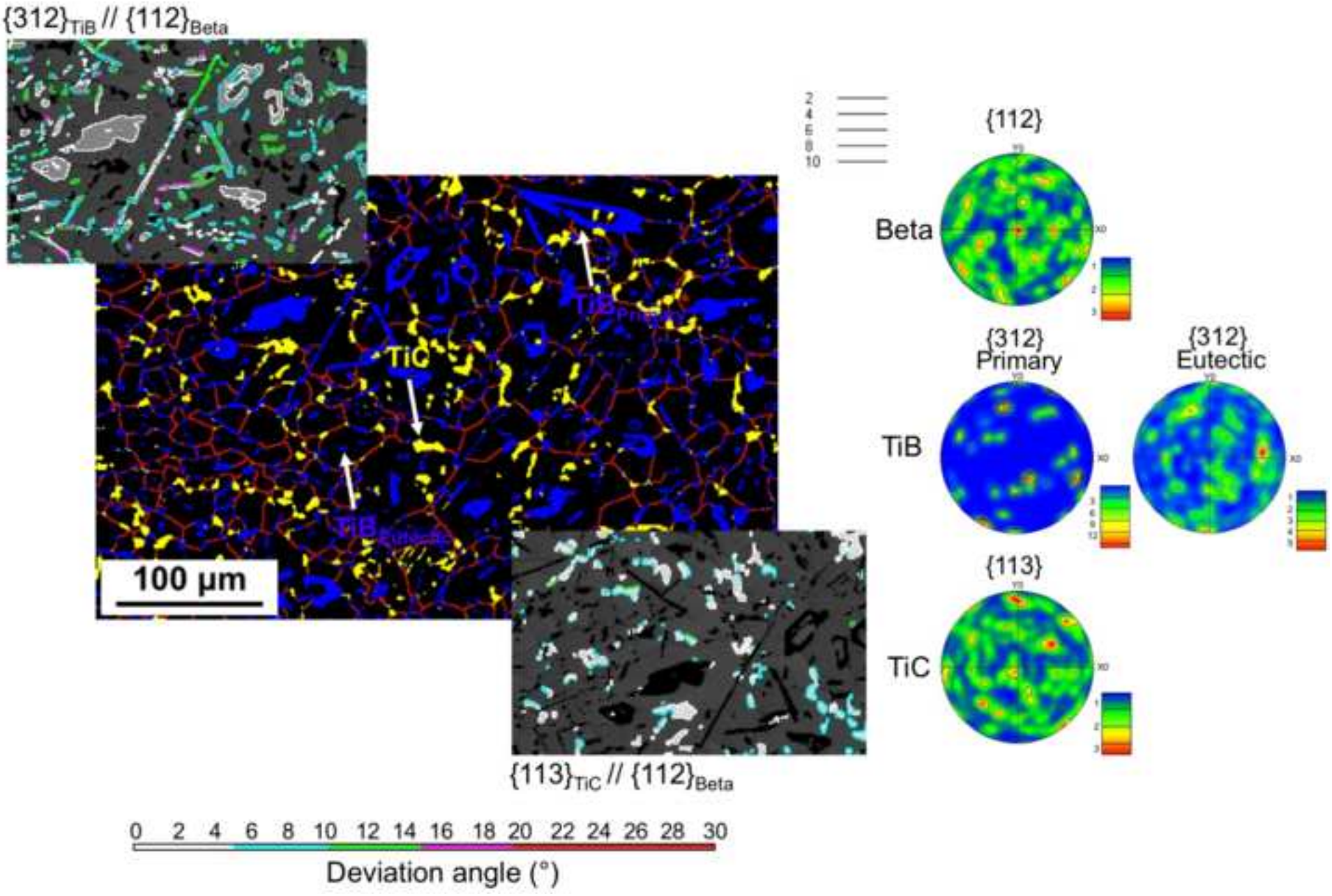

Figure 7
Click here to download high resolution image

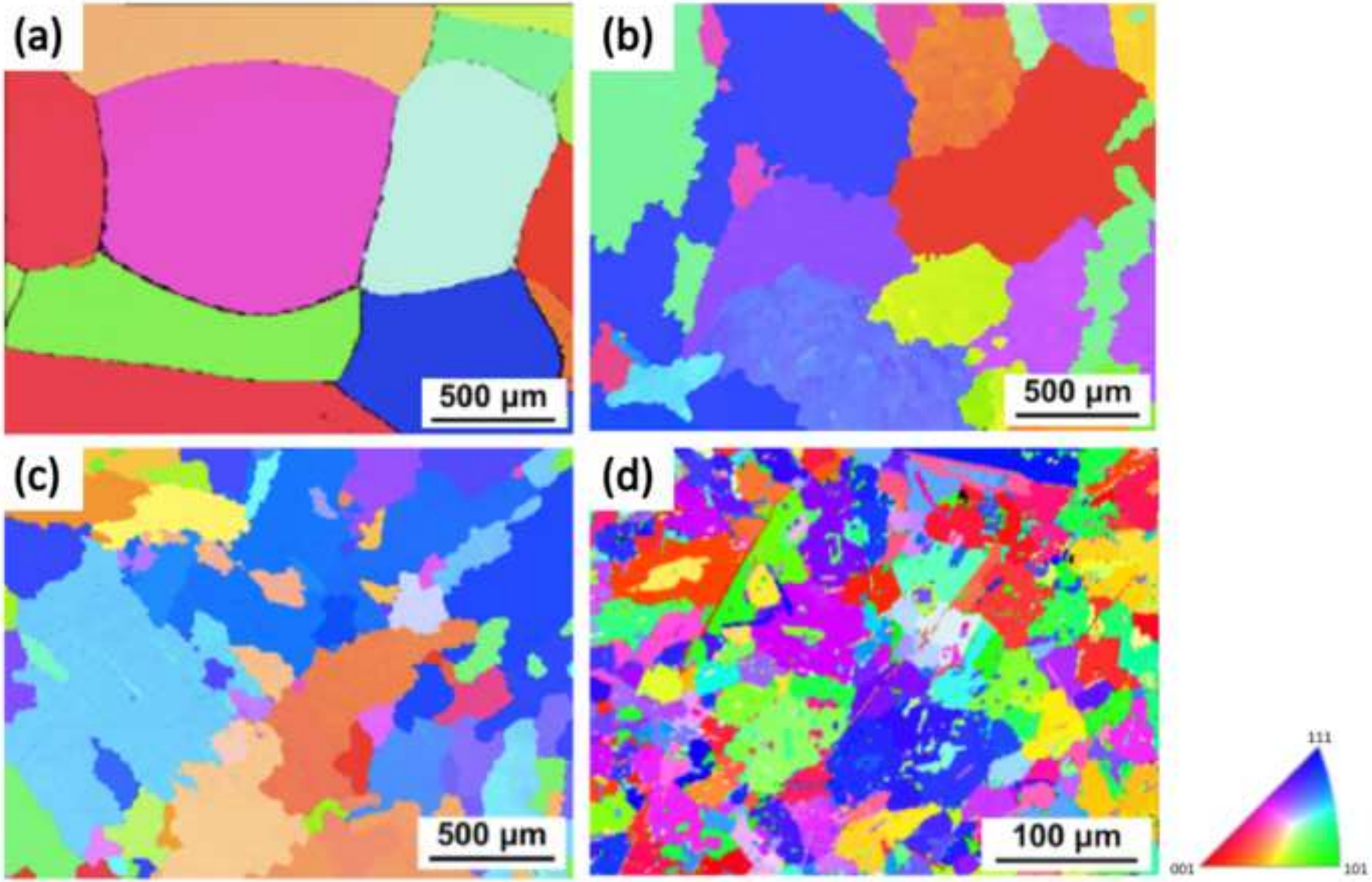

Figure 8

Click here to download high resolution image